ACTA IMEKO
ISSN: 2221-870X
September 2026, Volume 15, Number 3, 1 - 7

Monitoring of crack propagation in anisotropic rocks during compressive strength testing using gas permeability measurements

Martin Vavro[1], Leona Vavro[1], Lukáš Kubina[1], Karel Sosna[2]

[1] *The Czech Academy of Sciences, Institute of Geonics, Studentská 1768/9, 708 00 Ostrava-Poruba, Czech Republic*
[2] *SG Geotechnika a.s., Geologická 988/4, 152 00 Praha 5 – Hlubočepy, Czech Republic*

ABSTRACT
Porosity and related fluid permeability are key parameters that influence a number of other physical and mechanical properties of rocks and therefore have an impact on their specific engineering uses. Porosity and permeability depend on the microstructure of the rock, mainly on the size distribution, shape, and mutual connectivity of the pores in the rock matter, but also on the degree of rock failure caused by the presence of microcracks. This close connection between the rock's permeability and the presence of a microcrack network in the rock means, in other words, that changes in permeability during loading can serve as a measure for monitoring crack initiation and propagation. In the presented research, biotite migmatite, a metamorphic rock with a well-developed plane-parallel structure, was used for this purpose with the aim of simultaneously assessing the influence of textural anisotropy on the process of crack formation and development. It was found that an increase in gas permeability due to the formation of microcracks occurs when ca. 60 to 90 % of the maximum loading force is achieved, mostly depending on the spatial relationship between the orientation of anisotropy planes and the direction of the applied loading force.

Section: RESEARCH PAPER

Keywords: rock microstructure; gas permeability; triaxial compression test; crack propagation; failure process

Citation: M. Vavro, L. Vavro, L. Kubina, K. Sosna, Monitoring of crack propagation in anisotropic rocks during compressive strength testing using gas permeability measurements, Acta IMEKO, vol. 15 (2026) no. 3, pp. 1-7. DOI: 10.21014/actaimeko.v15i3.2476

Section Editor: Daniel Kytyr, Czech Academy of Sciences, Czechia

Received July 29, 2026; **In final form** September 7, 2026; **Published** September 2026

Funding: This research was financially supported by the project CZ.02.01.01/00/23_020/0008487 (INODIN), co-funded by the European Union and the project of the Czech Academy of Sciences – Strategy AV21, Research program: Dynamic Planet Earth (2023-2027).

Corresponding author: Martin Vavro, e-mail: martin.vavro@ugn.cas.cz

1. INTRODUCTION

Pore microstructure in rocks and similar rock-like geomaterials refers to the internal geometry, size distribution, volume, shape, orientation, connectivity and overall spatial arrangement of empty spaces—pores and cracks. It has a significant influence on many macroscopically observed and measured properties, such as rock strength, and its deformation, and fracture behaviour [1]–[4]. It also significantly influences fluid transport and storage capacity and co-determines rock resistance to weathering. Together with related rock permeability, it is therefore the crucial factor in assessing the suitability of rock host environment in such challenging engineering fields as the geological disposal of high-level radioactive waste or carbon sequestration in geological formations [5]-[9].

Monitoring of crack development is also of great importance in rock engineering. The presence of cracks in rocks and rock mass strongly affects, for example, the stability of underground workings, tunnels, or open pit slopes. Knowledge about crack propagation can also be applied in the prediction of anomalous geomechanical phenomena, such as rock bursts or rock and gas outbursts, or in the evaluation of rock fragmentation processes, such as drilling, blasting, crushing, and cutting [10], [11]. Cracks in rocks initiate and propagate in response to the applied stress, with the crack path often controlled by the microstructure and local distribution of microdefects such as cavities, inclusions, fossils, grain boundaries, mineral cleavage planes, etc. inside the rock [12]–[14]. Another factor that significantly influences the development of cracks is the anisotropy of rock fabric, manifested by the presence of bedding or foliation planes [15].

From the above, it is obvious that permeability reflects not only the petrography, microstructure, and physical properties of the rock, but also depends on the intensity of rock failure [16]–[18]. Permeability can be defined as the ability of a material to allow the passage of a fluid. In contrast with porosity, it is a vector quantity and depends not only on the filtration properties of the rock (its structure, particle size, density, porosity, etc.), but also on the physical properties of the liquid, especially viscosity [19]. Two different phases are very well distinguishable throughout the rock permeability evolution during the whole stress-strain process. In the first stage, permeability decreases as a result of axial compression, due to closure of the rock pore space. In the second phase, microcracks develop in the test specimen, which represent important paths for the passage of the filtration media, thus the rock permeability increases. Finally, when the tested rock fails, the increase in permeability is very high and can reach several times the initial permeability value [20]. This close relationship between the permeability of a rock to fluids and the state of the stress, or rather the degree of failure of the rock material, means that the change in permeability coefficient values during loading can be used as a very sensitive indicator for monitoring crack initiation, propagation, and growth within a test specimen.

To date, several advanced techniques have been adopted to study deformation and fracture processes in rocks subjected to different loading regimes (for overview, see, e.g., [21]). In this study, observations of gas permeability changes during compressive loading were made to indicate the moment of crack opening. Biotite migmatite, a metamorphic rock with very well-marked textural anisotropy, was used for the measurement. The main objective of the presented research was to verify whether continuously measured changes in rock permeability during loading can represent an alternative method for determining the stress level at which cracks begin to initiate and propagate in the rock. Another goal was to determine to what extent and in what way the anisotropy of the rock affects the formation and development of cracks under loading.

2. ROCK MATERIAL AND TEST SPECIMENS USED FOR EXPERIMENT

Medium-grained biotite migmatite with plane-parallel structure and lepidogranoblastic texture was used as a testing rock material. Distinct metamorphic foliation is expressed by the alternation of light and dark bands in the rock.

Light-coloured bands are formed by leucosome with varying proportions of felsic minerals, such as quartz, plagioclase, and K-feldspar. Dark bands of melanosome are composed of biotite flakes oriented parallel to the foliation (Figure 1). Biotite is locally altered to chlorite. Zircon, monazite, and apatite occur as accessory minerals.

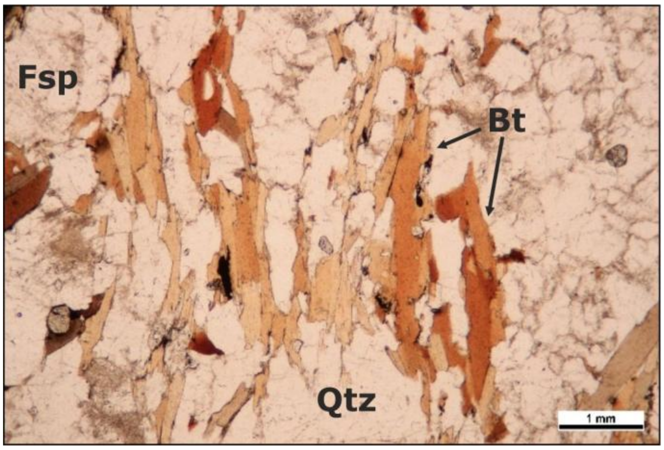

Figure 1. Micrograph of migmatite thin section showing preferred orientation of biotite flakes in the direction of metamorphic foliation (plane-polarised light, Qtz - quartz, Fsp - feldspar, Bt – biotite, photo M. Bošková).

The rock blocks for the preparation of test specimens were taken at level 22 of the former Rožná I uranium mine, i.e. from the depth of approximately 1100 meters below the Earth's surface. The tested migmatites represent one of the petrographic types forming the rock host environment of the Bukov Underground Research Facility (URF), which was gradually built at the Rožná I mine between 2013 and 2024 [22]–[24]. Bukov URF was created as a generic test site and represents a part of a national programme of the Radioactive Waste Repository Authority of the Czech Republic for planning a deep geological repository of high-level radioactive waste [5].

To measure rock permeability during loading, standard test specimens with a diameter of 48 mm and length of 96 mm, i.e. with the length-to-diameter (slenderness) ratio of 2.0, were drilled from the migmatite blocks. Core drilling was carried out in three directions to the metamorphic foliation—perpendicular (test samples marked as “K”), parallel (“P”), and oblique (ca. 30–60°, marked as “S”), see Figure 2. Basic physical and mechanical properties of the studied migmatite in relation to rock fabric anisotropy are presented in Table 1 and Table 2.

As is evident from Table 1 and Table 2, textural anisotropy, expressed by the presence of foliation planes, has a fundamental influence on the values of many physical and mechanical

Table 1. Average values of selected physical properties of rocks used for the experiment [25].

Property	Value	Property	Value
Mass density in kg·m^{-3}	2767	Thermal capacity - K in MJ·m^{-3}·K^{-1}	2.08
Bulk density in kg·m^{-3}	2742	Thermal capacity - P in MJ·m^{-3}·K^{-1}	2.25
Total porosity in %	0.67	Thermal capacity - S in MJ·m^{-3}·K^{-1}	1.99
Open porosity in %	0.39	Thermal diffusivity - K in mm·s^{-1}	1.18
Water absorption capacity in %	0.10	Thermal diffusivity - P in mm·s^{-1}	1.34
Ultrasonic wave velocity - K in km·s^{-1}	3.50	Thermal diffusivity - S in mm·s^{-1}	1.35
Ultrasonic wave velocity - P in km·s^{-1}	5.49	Thermal expansion - K in K^{-1}	$9.3 \cdot 10^{-6}$
Ultrasonic wave velocity - S in km·s^{-1}	4.48	Thermal expansion - P in K^{-1}	$8.7 \cdot 10^{-6}$
Thermal conductivity - K in W·m^{-1}·K^{-1}	2.47	Abrasiveness (CAI) - K	4.55
Thermal conductivity - P in W·m^{-1}·K^{-1}	3.00	Abrasiveness (CAI) - P	4.46
Thermal conductivity - S in W·m^{-1}·K^{-1}	2.69	Abrasiveness (CAI) - S	4.29

Note: All properties were determined on dried test samples, abrasiveness was determined by the CERCHAR method.

Table 2. Average values of selected mechanical and deformation properties of rocks used for the experiment [25].

Property	Value
Uniaxial compressive strength - K in MPa	165
Uniaxial compressive strength - P in MPa	126
Uniaxial compressive strength - S in MPa	74
Young’s modulus - K in GPa	41.0
Young’s modulus - P in GPa	53.9
Young’s modulus - S in GPa	29.5
Poisson’s ratio - K	0.17
Poisson’s ratio - P	0.16
Poisson’s ratio - S	0.12
Brazilian tensile strength - tension ⊥ to foliation in MPa	7.8
Brazilian tensile strength - tension // to foliation in MPa	12.7
Brazilian tensile strength - tension 45° to foliation in MPa	10.4

Note: All properties were determined on dried test samples.

Figure 2. Test specimens with a slenderness ratio of 2:1, drilled in three different directions (K, P, and S) in relation to the metamorphic foliation (left – K specimen, in the middle – P specimen, right – S specimen).

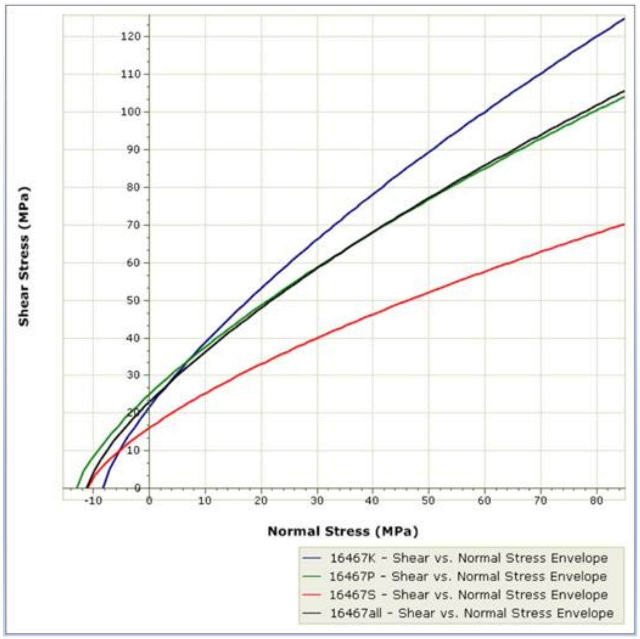

Figure 3. Different shape of strength envelopes for K, P, and S directions constructed according to the Hoek–Brown failure criterion in RocData software (Rocscience Inc.).

properties. In particular, there are different ultrasonic wave velocities, thermal properties, uniaxial compressive strength, Young’s moduli, and splitting (Brazilian) tensile strength in the K, P, and S directions. The influence of anisotropy on mechanical properties is then manifested in the different shape of failure envelopes, derived from the Hoek–Brown failure criterion [26] (Figure 3).

3. MEASURING EQUIPMENT AND METHODOLOGY OF THE EXPERIMENT

The main part of the laboratory equipment for measuring the gas permeability of rocks is represented by a KTK 100 triaxial cell (UNIPRESS, Poland) modified for gas passage. Basically, it is the so-called “false triaxial apparatus”, where the confining pressure ($\sigma_2 = \sigma_3$) is applied to the test specimen through hydraulic oil pressure, which, with the current design of the device, can reach a value of up to 30 MPa. The source of axial stress (σ_1) is a computer-controlled mechanical press ZWICK 1494 (Zwick/Roell, Germany) with the maximum force of 600 kN. Nitrogen is used as the gas medium for permeability measurements. Due to its properties and the short duration of the experiment, nitrogen can be considered an inert gas that does not react with the rock material.

The setup allows two measurement methods: (1) permeability measurement during increasing hydrostatic (confining) pressure and (2) permeability measurement under increasing axial stress. For the purposes of the presented experiment, the measurement mode at constant confining pressure and increasing axial stress was applied.

Before measurement, the test specimen was covered with a rubber membrane, then clamped in the jaws of the press machine, and the confining pressure was set to the value of 3 MPa. Subsequently, the axial stress was gradually increased by the movement of the press jaws ($\sigma_1 > \sigma_2 = \sigma_3$) up to the failure of the test specimen. Throughout the experiment, the nitrogen pressure was regulated from the gas pressure vessel using the control valve, to be continuously maintained at 3 MPa. The volume of passed gas was measured by a flow meter, at regular intervals of axial force increments of 5 kN. Gas permeability was calculated using Darcy’s law. A diagram showing the measuring equipment is shown in Figure 4.

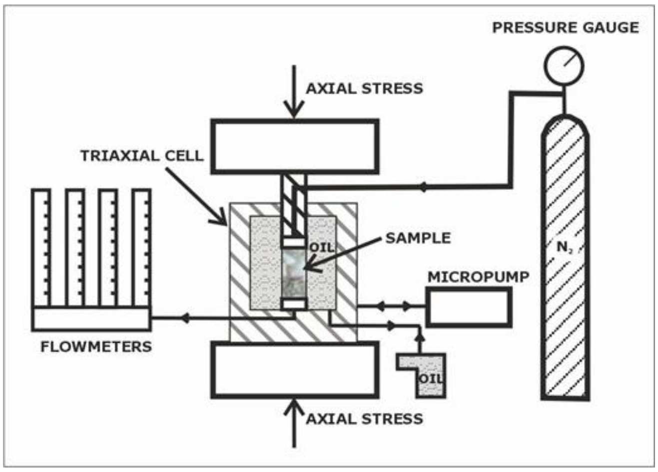

Figure 4. Diagram of the equipment for measuring gas permeability.

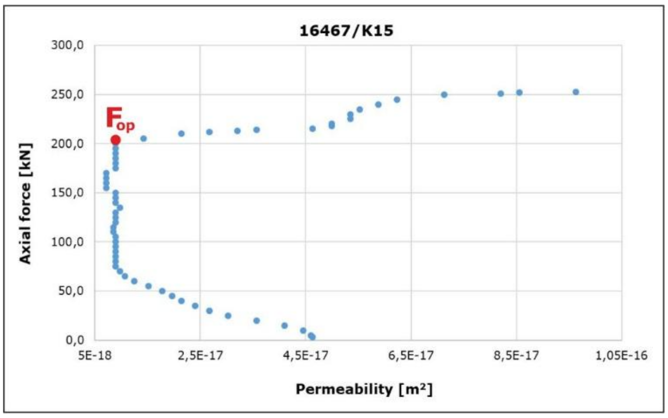

Figure 5. Typical course of gas permeability dependence on increasing loading force for test specimen K (F_{op} – crack opening force).

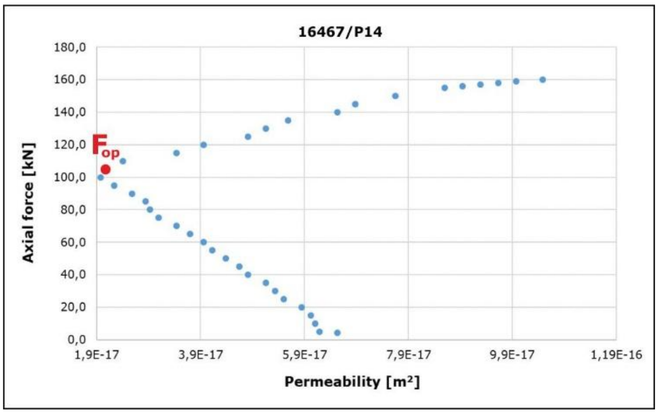

Figure 6. Typical course of gas permeability dependence on increasing loading force for test specimen P (F_{op} – crack opening force).

4. EXPERIMENTAL RESULTS

The results of the measuring gas permeability of rocks during loading, with the aim of using gas permeability as an indicator of the moment from which the crack begins to propagate, are shown in Figure 5 to Figure 7. Overall evaluation of measurement results, in the form of determining the level of the loading force required for crack initiation and propagation, is presented in Table 3.

The beginning of the crack initiation and subsequent propagation was identified based on a significant change in gas permeability evolution during a progressive failure process. As is visible from experimental curves in Figure 5 to Figure 7, the beginning of the crack formation is situated at the moment of an increase in gas permeability, which follows a previous continuous decrease of permeability, or a phase where the permeability is kept almost constant. The accuracy of determining this crack opening point corresponds to a loading force value of 5 kN, which is the interval of reading the amount of gas passing through the flow meter (see Chapter 3).

From Figure 5, it is obvious that for the presented test specimen 16467/K15 there is an evident time lag between the phases of decrease and increase in gas permeability during compressive loading. This course of gas permeability under loading is characteristic for all test specimens prepared in K direction.

Figure 6 shows the gas permeability during the pressure loading process for the selected test specimen 16467/P14. The course of changes in gas permeability values is different from the behaviour observed for test specimens K. A common feature of all tested P specimens, not only sample 16467/P14, is a gradual decrease in gas permeability during loading, in connection with the closure of the pore space, which is followed by an immediate increase in permeability due to the development of cracks.

As can be seen from Figure 7, for test specimens prepared in the S direction, both types of gas permeability changes during loading were observed, characteristic of both K specimens (gap between decreasing and increasing phases) and P specimens (immediate increase after a previous decrease in permeability).

For each tested migmatite specimen, the values of the maximum loading force at rock failure (F_{max}) and the force at which a significant increase in gas permeability occurred thanks to the formation of microcracks due to compression loading (F_{op}) are presented in Table 3.

In this context, it is necessary to draw attention to the fact that a different number of test specimens were tested in each of the K, P, and S directions. In the K and S directions, there were 7 and 8 specimens, respectively, while in the P direction, 4 specimens were evaluated. The reason was the quantity, size, and texture of the rock blocks that were available for the preparation of the test specimens. The number of tested samples can be considered sufficient for comparison of the three different specimen orientations, especially if this is an initial study on this issue.

It is evident from the data presented in Table 3 that the significant increase in gas permeability of the migmatite test

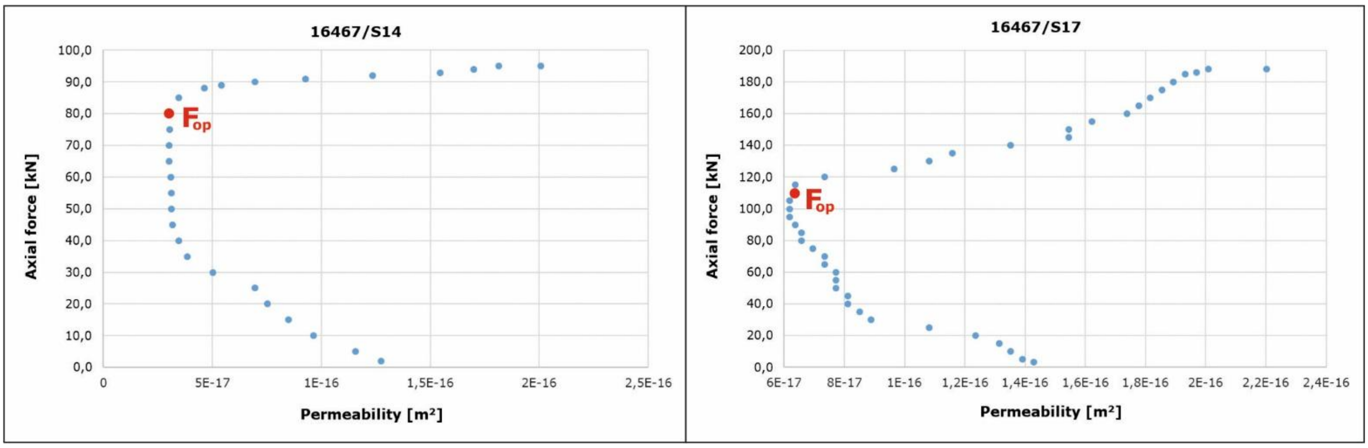

Figure 7. Two different courses of gas permeability dependence on increasing loading force identified for test specimens S (F_{op} – crack opening force).

Table 3. Comparison of maximal loading force and crack opening force for all tested migmatite specimens.

Direction	Test specimens	F_{max} in kN	F_{op} in kN	F_{op}/F_{max}	F_{op}/F_{max} - mean
K	16467/K14	247	180	0.73	0.79
	16467/K15	252	205	0.81	
	16467/K16	264	220	0.83	
	16467/K17	318	245	0.77	
	16467/K18	292	215	0.74	
	16467/K19	227	190	0.84	
	16467/K20	305	250	0.82	
P	16467/P14	160	105	0.66	0.65
	16467/P15	225	140	0.62	
	16467/P16	168	115	0.69	
	16467/P17	183	120	0.66	
S	16467/S13	175	140	0.80	0.78
	16467/S14	95	80	0.84	
	16467/S15	126	85	0.68	
	16467/S16	157	145	0.92	
	16467/S17	188	115	0.61	
	16467/S18	136	110	0.81	
	16467/S19	123	110	0.89	
	16467/S20	92	60	0.65	

specimens was found when approximately 60–90 % of F_{max} was reached. At the same time, there are significant differences in the behavior of test specimens K, P, and S during loading. In the case of K specimens, the ratio between crack opening force and maximal force ranges in a narrow interval of 0.73 to 0.84 with an average value of 0.79, standard deviation of 0.04 and coefficient of variation of 5.6 %. Also, in the case of test specimens in the P direction, the values of F_{op}/F_{max} ratio show very little dispersion, however, from 0.62 to 0.69 with an average value of 0.65. The average value of the F_{op}/F_{max} ratio for test specimens S (0.78) is almost the same as for the K direction (0.79), but the partial values are in a broad range between 0.61 and 0.92. This is reflected in higher values of standard deviation (0.12) and coefficient of variation (14.8 %) for the S direction. The research conducted to date has shown that crack initiation, leading to final rock failure, occurs evidently first in P samples (F_{op} between ca. 60 % to 70 % of F_{max}) in terms of the time course of loading, while in K samples and also some S samples, at the level up to ca. 75 % to 90 % of F_{max}.

5. CONCLUSIONS

The main findings obtained during this initial study can be summarized as follows:

- It was found that a significant increase in gas permeability due to microcracks formation occurs at a level of approximately 60 to 90 % of the maximum loading force. This finding is fully consistent with published data obtained by other study methods for crystalline rocks, but also sediments, both for compression loading regime [27]–[30] and bending loading regime [31]–[36].
- At the same time, it has been proven that the anisotropy of the studied migmatites plays a very important role both in the course of gas permeability during loading and in the value of the loading force at which the crack begins to propagate. The authors plan to verify the findings obtained from this method in their future research, using other, currently more commonly used methods, such as a combination of X-ray micro-tomography and acoustic emission measurement [21]. Crack development assessment using gas permeability measurements in other types of anisotropic rocks are also being prepared in order to generalize the conclusions about the influence of anisotropy on crack propagation in rocks.
- In the case of migmatite test specimens prepared in the K direction, this moment occurs on average at about 80 % F_{max}, with a typically relatively long delay between the increase in gas permeability and the preceding reduction of the pore space. This type of gas permeability change as a function of increasing axial loading is very similar to that described, for example, in [37] for Eibenstock granite.
- For samples P prepared parallel to the foliation, an increase in gas permeability occurs immediately after the previous closure of the pore space, on average at approximately 65 % of the peak force.
- As regards samples prepared obliquely to the foliation (S direction), both types of gas permeability curves described for test specimens K and P occur during loading. According to our observation, the moment of crack opening in S test specimens depends on the combination of three basic factors: (1) the value of the anisotropy angle between the foliation planes and loading direction, (2) the continuity and shape of the foliation planes, and (3) the presence and amount of weak minerals (biotite in this case) on the foliation planes and thickness of the biotite-rich melanosome bands.

Conducted research has shown that measuring changes in the gas permeability coefficient during loading can, to some extent, represent an alternative to other methods of studying the rock failure process, such as the acoustic emission technique.

Like any other laboratory testing method, measuring gas permeability during loading for the purpose of monitoring crack propagation has its advantages, but also its limitations. The distinct advantage, for example compared to X-ray computed micro-tomography technique, is the possibility of using larger test specimens, which allows us to study a larger and therefore more representative volume of the rock. A possible limitation is currently a somewhat lower sensitivity of detecting the exact moment of crack initiation compared to, for example, the acoustic emission (AE) method. However, unlike the AE technique, in addition to the compressive strength, another technically important material parameter of the rock is obtained during the measurement, in the form of gas permeability.

From the point of view of possible practical applicability, this method could be used, for example, in geotechnical assessment of the quality of the host environment for the location of a deep geological repository of high-level waste, where rock mass jointing and rock matrix permeability represent one of the crucial limiting factors.

ACKNOWLEDGEMENT

This research was financially supported by the project CZ.02.01.01/00/23_020/0008487 (INODIN), co-funded by the European Union and the project of the Czech Academy of Sciences – Strategy AV21, Research program: Dynamic Planet Earth (2023-2027).

REFERENCES

[1] A. Sufian, A. R. Russell, Microstructural pore changes and energy dissipation in Gosford sandstone during pre-failure loading using X-ray CT, Int. J. Rock Mech. Min. Sci. 57 (2013), pp. 119–131. DOI: 10.1016/j.ijrmms.2012.07.021

[2] S. Zabler, A. Rack, I. Manke, K. Thermann, J. Tiedemann, N. Harthill, H. Riesemeier, High-resolution tomography of cracks, voids and micro-structure in greywacke and limestone, J. Struct. Geol. 30 (2008) 7, pp. 876–887. DOI: 10.1016/j.jsg.2008.03.002

[3] Y. Zhao, W. Qin, A. Jin, H. Wu, Z. Chen, Research and analysis of the impact of the pore structure on the mechanical properties and fracture mechanism of sandstone, Mater. Today Commun. 38 (2024), 107753. DOI: 10.1016/j.mtcomm.2023.107753

[4] J. B. Zhu, T. Zhou, Z. Y. Liao, L. Sun, X. B. Li, R. Chen, Replication of internal defects and investigation of mechanical and fracture behaviour of rock using 3D printing and 3D numerical methods in combination with X-ray computerized tomography, Int. J. Rock Mech. Min. Sci. 106 (2018), pp. 198–212. DOI: 10.1016/j.ijrmms.2018.04.022

[5] Z. Bukovská, I. Soejono, L. Vondrovic, M. Vavro, K. Souček, D. Buriánek, P. Dobeš, O. Švajgera, (+ 9 more authors), Characterization and 3D visualization of underground research facility for deep geological repository experiments: A case study of underground research facility Bukov, Czech Republic, Eng. Geol. 259 (2019), 105186. DOI: 10.1016/j.enggeo.2019.105186

[6] J. Delay, P. Bossart, L. X. Ling, I. Blechschmidt, M. Ohlsson, A. Vinsot, C. Nussbaum, N. Maes, Three decades of underground research laboratories: what have we learnt?, Geol. Soc. London Spec. Publ. 400 (2014), pp. 7–32. DOI: 10.1144/SP400.1

[7] Y. Liu, P. Wang, M. Yang, Y. Zhao, J. Zhao, Y. Song, CO_2 sequestration in depleted methane hydrate sandy reservoirs, J. Nat. Gas Sci. Eng. 49 (2018), pp. 428–434. DOI: 10.1016/j.jngse.2017.10.023

[8] M. G. Rezk, J. Foroozesh, D. Zivar, M. Mumtaz, M., CO_2 storage potential during CO_2 enhanced oil recovery in sandstone reservoirs, J. Nat. Gas Sci. Eng. 66 (2019), pp. 233–243. DOI: 10.1016/j.jngse.2019.04.002

[9] D. Řimnáčová, Z. Weishauptová, O. Přibyl, I. Sýkorová, M. René, Effect of shale properties on CH_4 and CO_2 sorption capacity in Czech Silurian shales, J. Nat. Gas Sci. Eng. 80 (2020), 103377. DOI: 10.1016/j.jngse.2020.103377

[10] ISRM Commission on Testing Methods (F. Ouchterlony, co-ordinator), Suggested methods for determining the fracture toughness of rock, Int. J. Rock Mech. Min. Sci. & Geomech. Abst. 25 (1988) 2, pp. 71–96.

[11] B. N. Whittaker, R. N. Sing, G. Sun, Rock fracture mechanics: principles, design and applications, Elsevier Science Publishers B.V., Amsterdam, The Netherlands, 1992, ISBN 978-0444896841.

[12] R. Cao, P. Cao, H. Lin, X. Fan, Ch. Zhang, T. Liu, Crack initiation, propagation, and failure characteristics of jointed rock or rock-like specimens: A review, Adv. Civ. Eng. (2019), 6975751. DOI: 10.1155/2019/6975751

[13] A. Spetz, R. Denzer, E. Tudisco, O. Dahlblom, Phase-field fracture modelling of crack nucleation and propagation in porous rock, Int. J. Fract. 224 (2020) 1, pp. 31–46. DOI: 10.1007/s10704-020-00444-4

[14] L. Vavro, L. Malíková, P. Frantík, P. Kubeš, Z. Keršner, M. Vavro, An advanced assessment of mechanical fracture parameters of sandstones depending on the internal rock texture features, Acta Geodyn. Geomater. 16 (2019) 2, pp. 157–168. DOI: 10.13168/AGG.2019.0013

[15] Z. Aliabadian, G. F. Zhao, A. R. Russell, Crack development in transversely isotropic sandstone discs subjected to Brazilian tests observed using digital image correlation, Int. J. Rock Mech. Min. Sci. 119 (2019), pp. 211–221. DOI: 10.1016/j.ijrmms.2019.04.004

[16] W. Luo, Y. P. Qin, M. M. Zhang, C. X. Wang, Y. R. Wang, Test study on permeability properties of the sandstone specimen under triaxial stress condition, Procedia Eng. 26 (2011), pp. 173–178. DOI: 10.1016/j.proeng.2011.11.2156

[17] Y. Yang, Y. Song, S. Chen, Test study on permeability properties of coal specimen in complete stress-strain proces, Yantu Lixue/Rock Soil Mech. 28 (2007), pp. 381–385.

[18] Y. Zhao, H. Konietzky, T. Frühwirt, H. W. Zhou, Gas permeability evolution of coal with inclusions under triaxial compression – Lab testing and numerical simulations, Materials 15 (2022), 8567. DOI: 10.3390/ma15238567

[19] M. Vavro, K. Souček, L. Vavro, L. Georgiou, J. Mrógala, Study of the microstructure and permeability of building stone using X-ray micro-tomography, Period. Polytech.: Civ. Eng. 70 (2026) 1, pp. 11–27. DOI: 10.3311/PPci.42434

[20] X. Wang, H. Zhou, L. Zhang, A. Preusse, S. Xie, W. Hou, Research on damage-based coal permeability evolution for the whole stress-strain process considering temperature and pore pressure, Geomech. Geophys. Geo-Energy Geo-Resour. 8 (2022) 5, 149. DOI: 10.1007/s40948-022-00464-5

[21] D. Kytýř, P. Koudelka, D. Drozdenko, M. Vavro, T. Fíla, V. Rada, L. Vavro, K. Máthis, (+ 1 more author), Acoustic emission and 4D X-ray micro-tomography for monitoring crack propagation in rocks, Int. J. Rock Mech. Min. Sci. 183 (2024), 105917. DOI: 10.1016/j.ijrmms.2024.105917

[22] M. Vavro, K. Souček, L. Staš, P. Waclawik, L. Vavro, P. Konicek, J. Ptáček, J., Application of alternative methods for determination of rock quality designation (RQD) index: a case study from the Rožná I uranium mine, Strážek Moldanubicum, Bohemian Massif, Czech Republic, Can. Geotech. J. 52 (2015) 10, pp. 1466–1476. DOI: 10.1139/cgj-2014-0377

[23] K. Souček, M. Vavro, L. Staš, L. Vavro, P. Waclawik, P. Konicek, J. Ptáček, L. Vondrovic, Geotechnical characterization of Bukov Underground Research Facility, Procedia Eng. 191 (2017), pp. 711–718. DOI: 10.1016/j.proeng.2017.05.236

[24] L. Gong, K. Soucek, P. Waclawik, M. Vavro, L. Stas, J. Nemcik, S. Ram, Modelling the sensitivity of underground space stability to the in situ stress uncertainties: case study at the Bukov underground research facility phase II (Rožná mine, Czechia). Acta Geodyn. Geomater. 18 (2021) 3, pp. 319–334. DOI: 10.13168/AGG.2021.0022

[25] Z. Bukovská, O. Švagera, T. Chabr, J. Leichmann, K. Sosna, K. Souček, M. Vavro, M. Zuna (+ 41 more authors), Získání dat

z hlubokých horizontů dolu Rožná – závěrečná zpráva (Technická zpráva SÚRAO č. 464/2020) – Data acqusition from the deep horizons of the Rožná mine – final report (RAWRA technical report Nb. 464/2020), Praha, Czech Republic, 2020 [in Czech]. Online [Accessed 14 July 2026].
https://surao.gov.cz/wp-content/uploads/2025/07/TZ464_2020_ENG.pdf

[26] E. Hoek, E. T. Brown, The Hoek–Brown failure criterion and GSI – 2018 edition, J. Rock Mech. Geotech. Eng. 11 (2019) 3, pp. 445–463.
DOI: 10.1016/j.jrmge.2018.08.001

[27] G. K. Zhang, H. B. Li, M. Y. Wang, X. F. Li, Crack initiation of granite under uniaxial compression test, J. Rock Mech. Geotech. Eng. 12 (2020) 3, pp. 656–666.
DOI: 10.1016/j.jrmge.2019.07.014

[28] M. Cai, P. K. Kaiser, Y. Tasaka, T. Maejima, H. Morioka, M. Minami, Generalized crack initiation and crack damage stress thresholds of brittle rock masses near underground excavations, Int. J. Rock Mech. Min. Sci. 41 (2004) 5, pp. 833–844.
DOI: 10.1016/j.ijrmms.2004.02.001

[29] M. Nicksiar, C. D. Martin, Crack initiation stress in low porosity crystalline and sedimentary rocks, Eng. Geol. 154 (2013), pp. 64–76.
DOI: 10.1016/j.enggeo.2012.12.007

[30] M. Petružálek, T. Lokajíček, T. Svitek, Z. Jechumtálová, P. Kolář, J. Šílený, Fracturing of migmatite by acoustoc emission and ultrasonic sounding, Rock Mech. Rock Eng. 52 (2019) 1, pp. 47–59.
DOI: 10.1007/S00603-018-1590-2

[31] W. K. Zietlow, J. F. Labuz, Measurement of the intrinsic process zone in rock using acoustic emission, Int. J. Rock Mech. Min. Sci. 35, 3 (1998), pp. 291–299.
DOI: 10.1016/S0148-9062(97)00323-9

[32] T. Backers, S. Stanchits, G. Dresen, Tensile fracture propagation and acoustic emission activity in sandstone: the effect of loading rate, Int. J. Rock Mech. Min. Sci. 42 (2005) 7–8, pp. 1094–1101.
DOI: 10.1016/j.ijrmms.2005.05.011

[33] Q. Lin, J. F. Labuz, Fracture of sandstone characterized by digital image correlation, Int. J. Rock Mech. Min. Sci. 60 (2013), pp. 235–245.
DOI: 10.1016/j.ijrmms.2012.12.043

[34] L. Vavro, K. Souček, D. Kytýř, T. Fíla, Z. Keršner, M. Vavro, Visualization of the evolution of the fracture process zone by transmission computed radiography, Procedia Eng. 191 (2017), pp. 689–696.
DOI: 10.1016/j.proeng.2017.05.233

[35] W. Li, F. U. A. Shaikh, L. Wang, Y. Lu, K. Wang, Z. Li, Microscopic investigation of rate dependence on three-point notched-tip bending sandstone, Shock Vib. (2019), 4525162.
DOI: 10.1155/2019/4525162

[36] D. Vavrik, P. Benes, T. Fila, P. Koudelka, I. Kumpova, D. Kytyr, M. Vopalensky, M. Vavro, L. Vavro, Local fracture toughness testing of sandstone based on X-ray tomographic reconstruction, Int. J. Rock Mech. Min. Sci. 138 (2021), 104578.
DOI: 10.1016/j.ijrmms.2020.104578

[37] X. Tan, H. Konietzky, T. Frűhwirt, Laboratory observation and numerical simulation of permeability evolution during progressive failure of brittle rocks, Int. J. Rock Mech. Min. Sci. 68 (2014), pp. 167–176.
DOI: 10.1016/j.ijrmms.2014.02.016